ACS APPLIED MATERIALS & INTERFACES

Research Article

www.acsami.org

Enhanced Field Emission Performance of Hierarchical ZnO/Si Nanotrees with Spatially Branched Heteroassemblies

Shasha Lv,[†] Zhengcao Li,*[,†,‡] Chienhua Chen,[†] Jiecui Liao,[†] Guojing Wang,[†] Mingyang Li,[†,§] and Wei Miao[‡]

[†]The State Key Laboratory of New Ceramics and Fine Processing, School of Materials Science and Engineering, [‡]Key Laboratory of Advanced Materials (MOE), School of Materials Science and Engineering, and [§]Department of Engineering Physics, Tsinghua University, Beijing 100084, China

ABSTRACT: Silicon nanorods (SiNRs) with a large interspace and regularly aligned structure were fabricated by combining silver-catalyzed etching with a polysterene (PS) sphere template, then a hydrothermal reaction was utilized to synthesize large-scale ZnO nanowires (NWs) on Si nanorods. Compared with the as-prepared SiNRs and ZnO NWs, the high-density ZnO NWs on SiNRs have exhibited predominant field emission (FE) characteristics with a low turn-on field of 2.18 V/μm and a high field enhancement factor of ~8100. The FE enhancement was attributed to highly crystallized ZnO NWs densely distributed on the surface of SiNRs, which can effectively increase emission site density, diminish screening effect, favor electron transfer due to band bending, and quickly transmit heat from the nanotrees to substrate. Our results indicate that ZnO/Si hierarchical structures might be an effective candidate for field emission cathode.

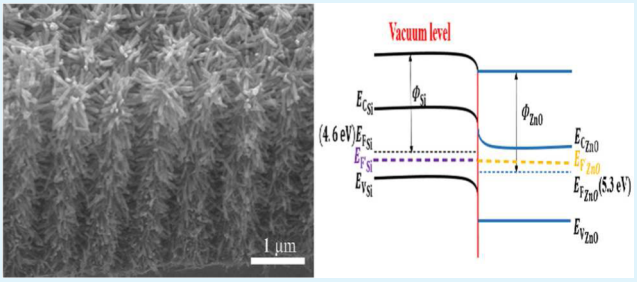

KEYWORDS: *silicon nanorods, ZnO nanowires, branched heterostructures, field emission, band bending*

INTRODUCTION

Three-dimensional (3D) nanoscale structures with modulated morphologies, compositions, and interfaces have attracted considerable attention. New modified heterostructures, such as graphene/ZnO NWs,[1] ZnO/MoS_2 nanoflowers,[2] and CdSe sheet/CdS NWs,[3] have potential applications for field emission cathodes. As compared to typical one-dimensional (1D) nanostructures, growing arrays on another individual 1D structure to form a 3D hierarchical nanostructure can increase surface area and improve charge transport.[4−6] In particular, nanotrees play an important role in FE field. Among these composites, two of the most studied semiconductors, Si and ZnO, have been chosen to form a spatially branched hierarchical system.[7]

Because of its abundance, stability, well-balanced electrical and optical properties, and highly developed microelectronic technology, silicon offers several advantages. These functional properties of Si-based nanostructures have stimulated widespread interest in field emission based devices,[8,9] such as flat-panel displays, parallel electron beam microscopes, and vacuum microwave amplifiers. But there are some disadvantages to the application of Si-based nanostructures, such as the oxidation of the surface during field emission, thereby degrading the performance of these devices.[10,11]

ZnO nanowires (NWs) have a large band gap, high exciton binding energy, and thermal stability,[12−14] which is useful as low-voltage FE devices.[15] Synthetic methodologies[16] (including hydrothermal reaction, template-assisted routing, vapor transport, electrospinning, etc.) have gradually been implemented of hierarchical ZnO nanostructures. Among these, hydrothermal synthesis provides a straightforward method for growing ZnO nanowires on arbitrary substrates in order to construct heterostructures.[17−19]

ZnO NWs could serve as a protecting layer for the SiNRs against environmental and ionization damage when employed in device fabrication. However, there has been few literature detailing the assemblied 3D ZnO/Si nanotrees for FE application. In the present study, hierarchical ZnO/Si nanotrees with spatially branched heteroassemblies were fabricated, and the factors leading to the enhanced FE current density were analyzed with respect to their unique morphological characteristics and band bending.

EXPERIMENTAL METHODS

The p-type (100) Si pieces were used as the substrate to assembly monodispersed PS nanosphere template as we reported before.[20] The diameter of PS sphere was reduced to get nonclose-packed hexagonal arrays by reactive ion etching (RIE) with an etching time of 300 s, O_2 flow rate of 40 sccm, basic pressure of 2 Pa, and applied radio frequency power of 30 W. After that, Ag film was deposited onto the Si substrate by magnetron sputtering, forming a porous Ag film as catalyzer. Subsequently, Si substrate with coated Ag film was etched in a mixture of deionized water, HF, and H_2O_2 at 30 °C for 8 min; and

Received: April 7, 2015
Accepted: June 3, 2015
Published: June 3, 2015

DOI: 10.1021/acsami.5b02976
ACS Appl. Mater. Interfaces 2015, 7, 13564−13568

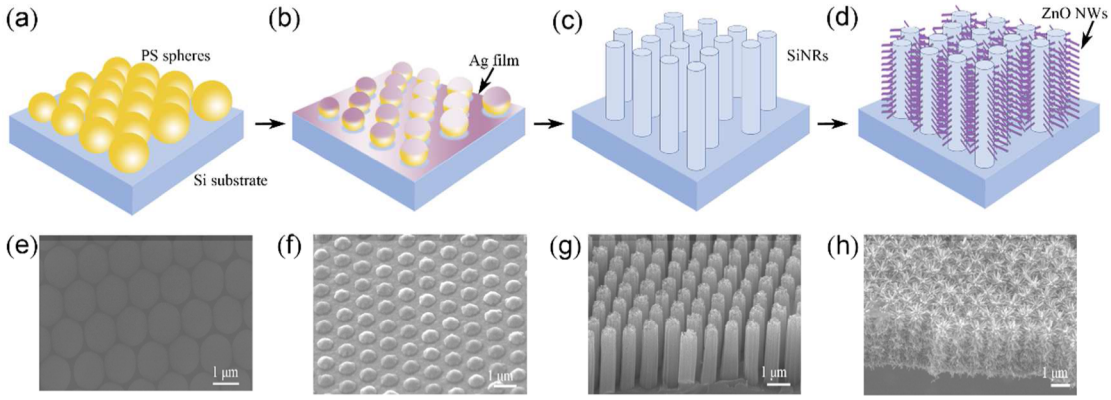

Figure 1. Schematic and FE-SEM images of synthesis of ZnO NWs/SiNRs.

the concentrations of HF and H_2O_2 were 4.8 and 0.3 M, respectively. At last, PS sphere templates and the retained Ag film were removed.

ZnO nanobranches were grown on the SiNRs by hydrothermal method. A seed solution of ZnO nanoparticles was prepared by 0.03 M NaOH and 0.01 M zinc acetate $[Zn(CH_3COO)_2]$ in methanol solution; then, the mixture was actively stirred at 60 °C for 2 h. Next, the seed solution was spin-coated onto silicon substrates with silicon nanorods (SiNRs), and the coating step was repeated for several times. ZnO nanowires were grown from the ZnO nanoparticle seeds through immersing in an precursor solution consisting of 25 mM zinc nitrate hydrate $[Zn(NO_3)_2{\cdot}6H_2O]$ and 25 mM hexamethylenetetramine ($C_6H_{12}N_4$, HMTA), heating, and stirring at 95 °C for 3 h. Finally, the samples were thoroughly rinsed with deionized water and then dried in air.

The morphology, microstructure, and composition of the heterostructures were observed by X-ray diffraction (XRD, Rigaku Smart Lab), field emission scanning electron microscopy (FE-SEM, JEOL-JSM 7001F, Tokyo, Japan), and transmission electron microscopy (TEM, JEOL-JSM 2011). The field emission properties of SiNRs were measured in a vacuum chamber with base pressures below 2×10^{-5} Pa. The samples were connected to the cathode. The phosphor was deposited on a transparent conductive material (indium−tin-oxide), to serve as the anode electrode in the vacuum system. The anode−cathode distance was kept constant with a thickness of 300 μm, and the measured emission area was $\sim 10 \times 10$ mm^2.

RESULTS AND DISCUSSION

Figure 1a−d and e−h show the schematic diagram of fabrication process of ZnO NWs/SiNRs hierarchical nanostructures and their correponding SEM images, respectively. A silver-catalyzed chemical etching approach that combines a PS sphere template with reactive ion etching (RIE) is used to fabricate well-aligned and large interspace nanorods. Panels a and e in Figure 1 show the typical hexagonal close-packed images of PS nanospheres, which have long-range order on the area of several centimeters squared. The diameter is reduced from 960 to 500 nm by RIE, and the spaces between the nanospheres can be utilized for the subsequent Ag film deposition with a thickness of 50 nm (Figure 1b, f). Panels c and g in Figure 1 exhibit the nanorods after metal catalytic etching are 3 μm in length and 500 nm in diameter, and they are well-separated and perpendicular to the sample surface, forming a regular aligned pillar arrays.[21] Then, by growing ZnO nanowires on individual SiNRs, nanoscale tree\-like nanocomposites with hierarchical architectures have been prepared (Figure 1d, h).

The morphology of ZnO nanowires can be controlled by modifying the seed-layer thickness and growth parameters. The samples of Figure 2a, b with different aspect ratios and densities of ZnO NWs is prepared by varying spin-coating cycles. Figure

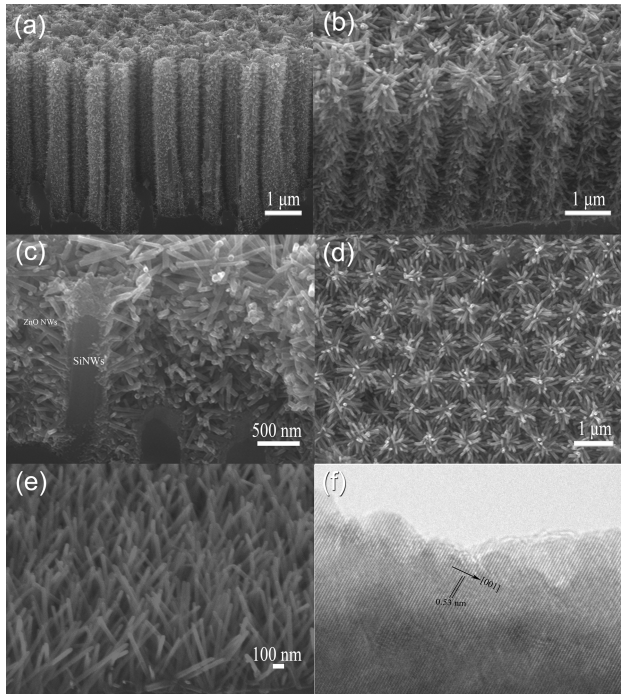

Figure 2. FE-SEM images of (a) sectional-view of low-density ZnO NWs/SiNRs, (b−d) sectional-view and top-view of high-density ZnO NWs/SiNRs, (e) ZnO NWs grown on planar silicon substrate, (f) HRTEM images of ZnO NWs grown on SiNRs.

2c, d shows top and cross-sectional SEM images of the sample of Figure 2b with high-density and large-aspect-ratio ZnO NWs on Si nanorods. The ZnO NWs grown densely on the top and lateral surface of SiNRs have a diameter of 50−90 nm and a length of 200−650 nm, and they exhibit different aspect ratios of 4−10, larger than aspect ratios of 2−5 of Figure 2a. In contrast, Figure 2e presents the ZnO NWs grown on silicon substrate with the same growing parameter of sample of Figure 2b, and they have a diameter of ∼70 nm and a length of ∼800 nm. The hydrothermal process to grow ZnO NWs on different substrates is all due to the accumulation and growth of ZnO molecules at a high concentration. However, ZnO NWs on Si wafers are much denser and longer than those grown on SiNRs, which indicates that accumulation of ZnO seeds can be

DOI: 10.1021/acsami.5b02976
ACS Appl. Mater. Interfaces 2015, 7, 13564−13568

efficiently controlled by introducing Si nanorod tree trunks. More importantly, when the SiNRs act as the nonplanar substrate, it can effectively relieve strain of large lattice mismatches, and control the site selective growth of ZnO NWs.[21] The TEM image (Figure 2f) shows that ZnO NWs have a preferential [001] orientation. The lattice spacing is approximately 0.52 nm, corresponding to the (001) crystal plane of ZnO.

The glancing angle X-ray diffraction (GIXRD) pattern of ZnO nanowires was taken to examine crystal structures. As shown in Figure 3, the peaks at 2θ = 31.4, 34.4, 36.3, 47.4, 56.6, and 62.8° originate from the (100), (002), (101), (102), (110), and (103) planes of ZnO, respectively. These signals show the hierarchical ZnO nanowires have a wurtzite structure with the lattice constants of a = 0.325 nm and c = 0.52 nm (JCPDS-ICDD Card No. 79−205).

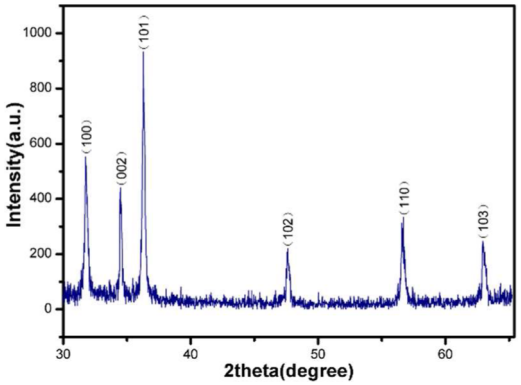

Figure 3. GIXRD spectrum of ZnO NWs grown on SiNRs.

Field emission is a quantum tunneling phenomenon whereby electrons are emitted from a solid surface into the vacuum in a strong electric field. During the FE process, the current density (J) produced by a given electric field (E) is described as the following equation[22]

$$J = \left(\frac{A\beta^2E^2}{\Phi}\right)\exp\left(-\frac{B\Phi^{3/2}}{\beta E}\right)$$

where $A = 1.54 \times 10^{-6}$ A eV V^{-2} and $B = 6.83 \times 10^3$ eV$^{-3/2}$ V μm^{-1}, β is the field enhancement factor, and Φ is the work function of emitters. Figure 4a displays the plot of current density related with electric field strength for SiNRs, ZnO NWs and ZnO/Si nanotrees. We observe negligible field emission currents from bare ZnO nanowires up to the maximum applied electric field. For a fixed applied field, it can be observed that the current density is enhanced by combining SiNRs with ZnO composite. The hybrid high-density ZnO NWs on SiNRs have lower turn-on field (E required for extracting a J of 10 μA/cm^2) of 2.18 V/μm than that of 3.68 V/μm for low-density ZnO NWs on SiNRs, and 5.20 V/μm for SiNRs. The result demonstrates that high-density and large-aspect-ratio ZnO nanobranches with SiNRs improve the FE properties significantly. The inset of Figure 4a shows the field emission images of high-density ZnO NWs on SiNRs operated at electric field of 4.2 V/μm. The light spots on the fluorescent screen are uniform and dense. The emission current−voltage characteristics were further analyzed by Fowler−Nordheim (F−N) equation (relationship between $\ln(J/E^2)$ and $1/E$) in Figure 4b, and the plot slope is equal to $-B\Phi^{3/2}\beta^{-1}$. For SiNRs, the F−N

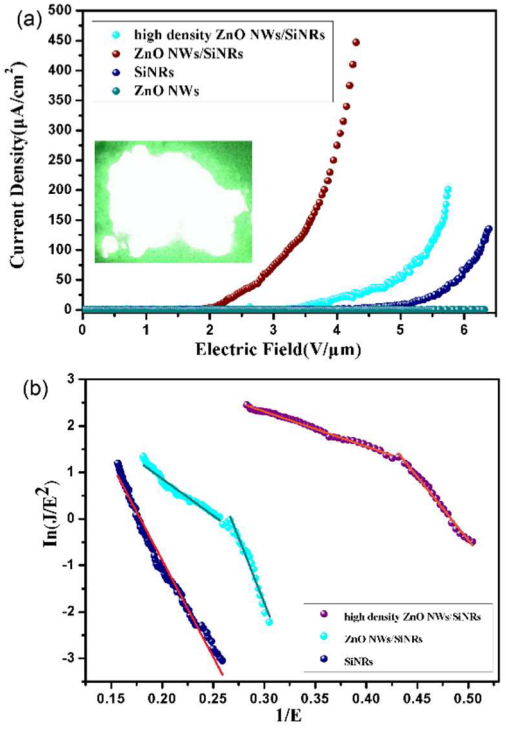

Figure 4. Field emission J−E plots of bare ZnO NWs, SiNRs, and ZnO NWs/SiNRs. (b) F−N plots for bare SiNRs and ZnO NWs/SiNRs.

plot show fit well to the linear relationship, which indicates that emission process are mostly due to vacuum tunneling. Taking Φ = 4.9 eV for SiNRs, the enhancement factor is estimated to be ∼1750. The relatively small aspect ratio of SiNRs is considered as a limitation to the FE property.

For the hybrid ZnO/Si nanotrees, the F−N plot displays a nonlinear relation in the low and high electric field range. A down bending F−N plot is usually observed for nanocomposites with electric field increasing, and it had been extensively discussed in many literatures. This increasing slope can be explained by the space charge effect, nonuniform geometries of emitters and the increasing emission sites with applied voltage increasing.[23] The calculated enhancement factors in the high electric field region (left part of plot) are found to be ∼8100 and 5260 for high-denity and low-density ZnO NWs, respectively, which is substantially higher than that for SiNRs.

The SiNRs capped with ZnO NWs can favor electrons emission by band bending, as described in Figure 5. The electrons transfer mechanism of the heterojunction is mainly

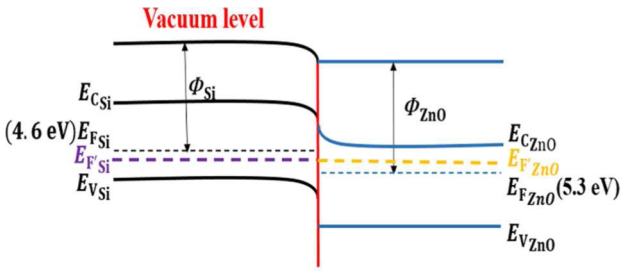

Figure 5. Schematic diagram for probable mechanism of FE property enhancement due to band bending.

DOI: 10.1021/acsami.5b02976
ACS Appl. Mater. Interfaces 2015, 7, 13564−13568

thermal emission caused by the different work function of materials. The work functions Φ of Si (4.9 eV) and ZnO (5.3 eV) differ by 0.4 eV, and the junction between Si and ZnO could level their dissimilar work function. When taking the electron affinities into account, the downhill potential between conduction bands of Si (4.01 eV) and ZnO (4.35 eV) is 0.34 eV. Therefore, the ZnO conduction band edge should be at a lower energy level compared to that of Si, which favors electrons transferring through the SiNRs−ZnO junction under low electric field.[21] Then, the electrons in the conduction band of ZnO are emitted to the vacuum through subsequent F−N tunneling under local electric field.

It is to be noted that only the difference of work function and electron affinities between Si and ZnO is insufficient to conclusively explain the enhancement of FE properties. The geometrical predominance of the hierarchical structure is considered as another reason. When two different sorts of nanostructures are combined, the total field enhancement factor is the combination of two individual nanostructures,[24] presented as. $\beta_{total} = \beta_{SiNWs}\beta_{ZnONWs}$ The increase in β value of heterostructures is greatly attributed to the geometrical factors such as aspect ratio, interspace between emitters, surface undulation, density of emitters, etc.[25] The high densities and large aspect ratios of ZnO NWs grown on the preformed SiNRs templates can increase the effective number of emission sites and lead to regular surface undulation, both of which are helpful for electrons emission and tunneling from the emitters. Such a geometrical configuration of ZnO/Si nanotrees would largely diminish the screening effect[26] and control the final space distribution[27] of heterostructure emitters. A comparison of FE properties of our results with the other published work on modified heterostructures is provided in Table 1. We can see that the turn-on field and β obtained in our study is better than most of the values, because of band bending and the abundance of emission sites together.

Table 1. Comparative Table of the Field Emission Properties of Modified ZnO NWs

sample	turn-on field	β
ZnO nanowires[28]	3.82 (0.1 μA/cm^2)	2303
ZnO pencils[29]	1.38 (0.1 μA/cm^2)	
ZnO nanobelts[30]	6.7 (10 μA/cm^2)	700
Al-doped ZnO NWs[31]	2.8 (10 μA/cm^2)	796
Au/ZnO nanopillars[7]	2.65 (10 μA/cm^2)	3313
graphene/ZnO[1]	5.4 (10 μA/cm^2)	1100
MoS_2 @ ZnO nanoflowers[2]	3.08 (10 μA/cm^2)	2839
SiNW−ZnO core−shell[32]	7.6 (1 μA/cm^2)	4227
ZnO NWs on SiNWs[6]	2.9 (10 μA/cm^2)	1311
ZnO/Si nanotrees in present work	2.18 (10 μA/cm^2)	8100

The emission stability of ZnO NWs/SiNRs was tested under a constant electric field of 3.5 V/μm, and no obvious degradation of FE current density was observed. The current density in Figure 6 was kept at ∼190 μA/cm^{-2}, and the emission current fluctuation was with 4.8% during 180 min, which exhibited high emission stability. The structure of highly crystallized ZnO nanowires grown on the SiNRs with a large contact area can quickly transmit heat from nanotrees to the substrate,[27] so that the ZnO nanostructures can be effectively protected from being destroyed because of the superheat. This stability test aslo prove that ZnO has excellent chemical stability and can protect the emitter from ion bombardment during operation.

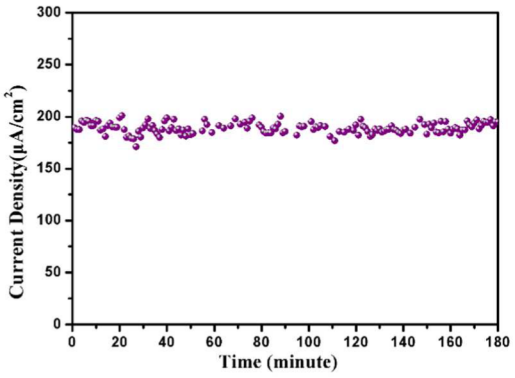

Figure 6. FE stability of ZnO NWs/SiNRs at an applied field of 3.5 V/μm.

CONCLUSION

We demonstrate a new and simple fabrication method for creating 3D nanotree-like ZnO/Si nanocomposites with a spatially branched hierarchical structure. In this approach, a combination of PS sphere template with metal-catalyzed etching is employed to fabricate regularly patterned and large interspace SiNRs. Then, by using a hydrothermal process, ZnO nanobranches are deposited onto preformed SiNRs. The hybrid high-density ZnO nanobranches on SiNRs have a lower turn-on field of 2.18 V/μm and a high field enhancement factor of ∼8100, Additionaly, FE properties with ZnO NWs, SiNRs and low-density ZnO nanobranches on SiNRs are aslo measured. The emission current stability test have also demonstrated the robustness of the ZnO/Si nanocomposites. The increment in FE property is caused by two phenomena: electronic band bending effect and the predominant geometrical morphology. The ohmic contact with nonrectifying barriers between silicon and ZnO determines the efficient electron flow from the SiNRs to the ZnO NWs. Furthermore, the high aspect ratios of ZnO NWs also act as independent emitters, magnify the electric field enhancement of SiNRs, improve the number of emitting dots, and diminish the screening effect. Therefore, it is expected that these 3D ZnO/Si nanocomposites will stimulate greater innovations for the application of field emission devices.

AUTHOR INFORMATION

Corresponding Author

*E-mail: zcli@tsinghua.edu.cn.

Notes

The authors declare no competing financial interest.

ACKNOWLEDGMENTS

The authors wish to thank Doctor Peng Liu from Tsinghua-Foxconn Nanotechnology Research Center for his kind advices and measurements to this work. The central laboratory of Institute of Materials Science and Engineering, Tsinghua University and the National Center for Electron Microscopy (Beijing) are also gratefully acknowledged for supporting the analysis and characterizing of the silicon nanowires in this work. The authors are grateful to the financial support by the Natural Science Foundation of China (61176003 and 61076003).

DOI: 10.1021/acsami.5b02976
ACS Appl. Mater. Interfaces 2015, 7, 13564−13568

REFERENCES

(1) Yang, Z. C.; Zhao, Q.; Ou, Y. X.; Wang, W.; Li, H.; Yu, D. P. Enhanced Field Emission from Large Scale Uniform Monolayer Graphene Supported by Well-aligned ZnO Nanowire Arrays. *Appl. Phys. Lett.* **2012**, *101*, 173107.

(2) Tan, Y. H.; Yu, K.; Li, J. Z.; Fu, H.; Zhu, Z. Q. MoS_2@ZnO Nano-heterojunctions with Enhanced Photocatalysis and Field Emission Properties. *J. Appl. Phys.* **2014**, *116*, 064305.

(3) Li, G. H.; Jiang, Y.; Zhang, Y. G.; Lan, X. Z.; Zhai, T. Y.; Yi, G. C. High-performance Photodetectors and Enhanced Field-emission of CdS Nanowire Arrays on CdSe Single-crystalline Sheets. *J. Mater. Chem. C* **2014**, *2*, 8252−8258.

(4) Cheng, C. W.; Yan, B.; Wong, S. M.; Li, X. L.; Zhou, W.; Yu, T.; Shen, Z. X.; Yu, H. Y.; Fan, H. J. Fabrication and SERS Performance of Silver Nanoparticles-Decorated Si/ZnO Nanotrees in Ordered Arrays. *ACS Appl. Mater. Interfaces* **2010**, *2*, 1824−1828.

(5) Ko, S. H.; Lee, D.; Kang, H. W.; Nam, K. H.; Yeo, J. Y.; Hong, S. J.; Grigoropoulos, C. P.; Sungl, H. J. Nanoforest of Hydrothermally Grown Hierarchical ZnO Nanowires for a High Efficiency Dye-Sensitized Solar Cell. *Nano Lett.* **2011**, *11*, 666−671.

(6) Wu, H. C.; Tsai, T. Y.; Chu, F. H.; Tai, N. H.; Lin, H. N.; Chiu, H. T.; Lee, C. Y. Electron Field Emission Properties of Nanomaterials on Rough Silicon Rods. *J. Phys. Chem. C* **2010**, *114*, 130−133.

(7) Chang, Y. M.; Lin, M. L.; Lai, T. Y.; Lee, H. Y.; Lin, C. M.; Wu, C. H. S.; Juang, J. Y. Field Emission Properties of Gold Nanoparticle-Decorated ZnO Nanopillars. *ACS Appl. Mater. Interfaces* **2012**, *4*, 6676−6682.

(8) Cui, Y.; Zhong, Z.; Wang, D.; Wang, W. U.; Lieber, C. M. High Performance Silicon Nanowire Field Effect Transistors. *Nano Lett.* **2003**, *3*, 149.

(9) Sun, X. Z.; Tao, R.; Lin, L. H.; Li, Z. C.; Zhang, Z. J.; Feng, J. Y. Fabrication and Characterization of Polycrystalline Silicon Nanowires with Silver-assistance by Electroless Deposition. *Appl. Surf. Sci.* **2011**, *257*, 3861.

(10) Lv, S. S.; Li, Z. C.; Su, S. M.; Lin, L. H.; Zhang, Z. J.; Miao, W. Tunable Field Emission Properties of Well-aligned Silicon Nanowires with Controlled Aspect Ratio and Proximity. *RSC Adv.* **2014**, *4*, 31729−31734.

(11) Lin, L. H.; Li, Z. C.; Zhang, Z. J.; Feng, J. Y. Direct Radiative Recombination in the Se-terminated Nanoscale Si Porous Structure. *Appl. Surf. Sci.* **2012**, *258*, 6977−6981.

(12) Wang, Z. L. Splendid One-dimensional Nanostructures of Zinc Oxide: A New Nanomaterial Family for Nanotechnology. *ACS Nano* **2008**, *2*, 1987−1992.

(13) Zhan, P.; Xie, Z.; Li, Z. C.; Wang, W. P.; Zhang, Z. J.; Li, Z. X.; Cheng, G. D.; Zhang, P.; Wang, B. Y.; Cao, X. Z. Origin of the Defects-induced Ferromagnetism in Un-doped ZnO Single Crystals. *Appl. Phys. Lett.* **2013**, *102*, 071914.

(14) Cho, S.; Jang, J. W.; Lee, J. S.; Lee, K. H. Room Temperature Synthesis and Optical Properties of Small Diameter (5 nm) ZnO Nanorod Arrays. *Nanoscale* **2010**, *2*, 2199−2202.

(15) Yan, X. B.; Tay, B. K.; Miele, P. Field Emission from Ordered Carbon Nanotube-ZnO Heterojunction Arrays. *Carbon* **2008**, *46*, 753−758.

(16) Lee, M. Y.; Kwak, G. J.; Yong, K. J. Wettability Control of ZnO Nanoparticles for Universal Applications. *ACS Appl. Mater. Interfaces* **2011**, *3*, 3350−3356.

(17) Sugavaneshwar, R. P.; Nanda, K. K. Multistage Effect in Enhancing the Field Emission Behaviour of ZnO Branched Nanostructures. *Appl. Phys. Lett.* **2014**, *104*, 222104.

(18) Hwang, J. O.; Lee, D. H.; Kim, J. Y.; Han, T. H.; Kim, B. H.; Park, M.; No, K.; Kim, S. O. Vertical ZnO Nanowires/graphene Hybrids for Transparent and Flexible Field Emission. *J. Mater. Chem.* **2011**, *21*, 3432−3437.

(19) Xia, G. D.; Jeong, S. J.; Kim, J. E.; Kim, B. H.; Koo, C. M.; Kim, S. O. Spin Coating Nanopatterned Multielemental Materials via Self-assembled Nanotemplates. *Nanotechnology* **2009**, *20*, 225301.

(20) Su, S. M.; Lin, L. H.; Li, Z. C.; Feng, J. Y.; Zhang, Z. J. The Fabrication of Large-scale Sub-10-nm Core-shell Silicon Nanowire Arrays. *Nanoscale Res. Lett.* **2013**, *8*, 405.

(21) Das, N. S.; Banerjee, D.; Chattopadhyay, K. K. High Efficiency Electron Field Emission from Protruded Graphene Oxide Nanosheets Supported on Sharp Silicon Nanowires. *J. Mater. Sci.* **2013**, *48*, 750−757.

(22) Stern, T. E.; Gossling, B. S.; Fowler, R. H. Electron Emission in Intense Electric Fields. *Proc. R. Soc. London, Ser. A* **1929**, *124*, 699−723.

(23) Lu, X.; Yang, Q.; Xiao, C.; Hirose, A. Nonlinear Fowler−Nordheim Plots of the Field Electron Emission from Graphitic Nanocones: Influence of Non-uniform Field Enhancement Factors. *J. Phys. D: Appl. Phys.* **2006**, *39*, 3375−3379.

(24) Khanna, R.; Pearton, S. J.; Ren, F.; Kravchenko, I.; Kao, C. J.; Chi, G. C. W_2B-Based Rectifying Contact to n-GaN. *Appl. Phys. Lett.* **2005**, *87*, 052110.

(25) Lv, S. S.; Li, Z. C.; Liao, J. C.; Zhang, Z. J.; Miao, W. Well-aligned NiSi/Si Heterostructured Nanowire Arrays as Field Emitters. *J. Vac. Sci. Technol. B* **2015**, *33*, 02B101.

(26) Galléa, F.; Li, Z. C.; Zhang, Z. J. Growth Control of Tungsten Oxide Nanostructures on Planar Silicon Substrates. *Appl. Phys. Lett.* **2006**, *89*, 193111.

(27) Xu, H. J.; Chan, Y. F.; Su, L.; Li, D. Y.; Sun, X. M. Enhanced Field Emission from ZnO Nanowires Grown on a Silicon Nanoporous Pillar Array. *J. Appl. Phys.* **2010**, *108*, 114301.

(28) Chu, F. H.; Huang, C. W.; Hsin, C. L.; Wang, C. W.; Yu, S. Y.; Yeh, P. H.; Wu, W. W. Well-aligned ZnO Nanowires with Excellent Field Emission and Photocatalytic Properties. *Nanoscale* **2012**, *4*, 1471.

(29) Warule, S. S.; Chaudhari, N. S.; Ambekar, J. D.; Kale, B. B.; More, M. A. Hierarchical Nanostructured ZnO with Nanorods Engendered to Nanopencils and Pin-Cushion Cactus with Its Field Emission Study. *ACS Appl. Mater. Interfaces* **2011**, *3*, 3454−3462.

(30) Xing, G. Z.; et al. Ultrathin Single-crystal ZnO Nanobelts: Ag-catalyzed Growth and Field Emission Property. *Nanotechnology* **2010**, *21*, 255701.

(31) Hsu, C. L.; Sua, C. W.; Hsueh, T. J. Enhanced Field Emission of Al-doped ZnO Nanowires Grown on a Flexible Polyimide Substrate with UV Exposure. *RSC Adv.* **2014**, *4*, 2980−2983.

(32) Kale, V. S.; Prabhakar, R. R.; Pramana, S. S.; Rao, M.; Sow, C. H.; Jinesh, K. B.; Mhaisalkarab, S. G. Enhanced Electron Field Emission Properties of High Aspect Ratio Silicon Nanowire−Zinc Oxide Core−Shell Arrays. *Phys. Chem. Chem. Phys.* **2012**, *14*, 4614−4619.

DOI: 10.1021/acsami.5b02976
ACS Appl. Mater. Interfaces 2015, 7, 13564−13568